AIAA JOURNAL
Vol. 33, No. 8, August 1995

Experimental Investigation of Convecting Vortex/Boundary-Layer Interactions

Michael Macrorie* and Wayne R. Pauley†
Pennsylvania State University, University Park, Pennsylvania 16802

The interaction between propagating spanwise vortices and a turbulent boundary layer was studied experimentally. The results focus on the relationship between the passage of vortex structures and the response of the boundary layer in terms of ensemble-averaged unsteady mean velocity, wall shear, and turbulent stresses. Both positive and negative circulation vortices were studied at different heights above the test surface. The results indicate that the sign of the vortex has an effect on the wall shear response as well as the height of the vortex above the surface. The negative circulation vortices were found to interact more closely with and penetrate deeper into the boundary layer than the positive sense vortices. A phase lag between the freestream disturbance caused by the vortex and the wall shear stress response is demonstrated. The relationship of the measured wall-shear stress to the pressure gradient and to a scaling velocity determined from the standard log-law fit for the overlap layer are discussed. The response of the boundary-layer turbulence is examined at key phases during the interaction.

Nomenclature

c	= flap chord, 2 cm
t^*	= time elapsed after vortex generated
U_c	= convection speed
U_e	= boundary-layer edge velocity
U_∞	= freestream speed, 5.9 m/s
U, V	= ensemble-averaged velocity components corresponding to (x, y)
$\overline{u'^2}, \overline{v'^2}$	= ensemble-averaged normal stresses
$\overline{u'v'}$	= ensemble-averaged turbulent shear stress
x	= streamwise distance from leading edge
Y_f	= normalized flap height, (y/c)
y	= normal distance from test plate surface
δ_{99s}	= boundary-layer thickness for steady (undisturbed) flow
ξ	= nondimensional streamwise pressure gradient, $\delta_{99s}/\tau_w \, \partial p_e/\partial x$
τ_w	= wall shear stress, N/m^2

Introduction

MANY boundary layers of engineering interest develop under conditions in which the freestream contains significant disturbances. These disturbances often take the form of freestream vortical structures. These unsteady, or convecting, freestream disturbances cause undesirable effects such as structure vibration, noise, and unsteady skin friction and heat transfer. Unsteady freestream disturbances also cause significant modulation of the boundary-layer transition location.[1] Boundary layers developing under freestreams with high turbulence levels are known to have increased time-averaged skin friction and heat transfer.[2] Past experiments conducted to investigate the effects of freestreams with highly unsteady vortical structures have typically employed grids to generate turbulence, which then interacts with a flat plate test surface. In these freestream turbulence studies the measurements have focused on time-averaged boundary-layer development in terms of heat transfer, skin friction, and velocity field. A significant parameter has been identified, the ratio of a representative turbulence length scale to the boundary-layer thickness. The conclusion of many researchers is that the increases in skin friction caused by high freestream turbulence approach a limit as the length scale of the freestream turbulence increases. This has been interpreted to indicate that freestream turbulence loses its effectiveness due to damping of the wall-normal velocity when its length scale becomes of the order of the boundary-layer thickness.

Another class of experiments has investigated boundary layers subjected to one-dimensional periodic disturbances, recent examples being those of Brereton et al.[3] and Samson et al.[4] In these experiments the unsteady component of the freestream velocity varies in a purely time-dependent manner. Samson et al.[4] presented hot-wire measurements from a two-dimensional unsteady boundary-layer experiment at three reduced frequencies. They found significant departures from a quasisteady representation of the Reynolds stress amplitude and phase angle profiles. They concluded that quasisteady turbulence modeling in the reduced frequency range of their experiment would not be appropriate. A more complex freestream condition that has been studied is the traveling wave disturbance of Patel.[5] The traveling wave disturbance produces not only time-dependent but also spatially dependent disturbances in the freestream. Evans and Yip[6] reported on the response of a flat plate turbulent boundary layer to propagating wake structures generated by a rotating cage.

Although the general freestream turbulence problem is inherently three dimensional, the present investigation is focused on the representative problem of the response of a two-dimensional boundary layer to two-dimensional spanwise freestream vortical structures. This study is simplified in comparison to the general problem, but it contains the very important feature of unsteady flow normal to the wall. It is related to two recent experimental studies of spanwise vortex structures propagating near a solid surface. Nelson et al.[7] studied the flowfield behind an oscillating spoiler mounted on a wind-tunnel wall. The pitching spoiler caused the flow along the wall to separate and form a vortex, which they characterized in terms of velocity and vorticity fields, and wall pressure. Gursul and Rockwell[8] studied the interaction of a vortex street with an elliptical leading edge. They used a combination of flow-visualization, phase-averaged wall-pressure, and velocity-field measurements to identify different classes of vortex/leading-edge interactions.

In the present study, the experimental approach involved generating repeatable freestream vortical structures that are on the scale of the undisturbed boundary-layer thickness. Measurements of the time-dependent boundary-layer response are reported in terms of its two-dimensional outer velocity field (unsteady mean and turbulence) along with the near-wall streamwise velocity field and the wall shear. To resolve the unsteady flow, ensemble averaging is used. The vortices are generated in the freestream to separate the generation process from the development of the boundary layer. The

Presented as Paper 93-0552 at the AIAA 31st Aerospace Sciences Meeting, Reno, NV, Jan. 11–14, 1993; received July 10, 1993; revision received Nov. 14, 1994; accepted for publication Nov. 15, 1994.

*Research Assistant, Department of Aerospace Engineering; currently Engineer, GE Aircraft Engines, Lynn, MA 01910.

†Assistant Professor, Department of Aerospace Engineering. Member AIAA.

measurements are taken in a region where the undisturbed boundary-layer is fully developed and the vortices have sufficient strength to cause severe distortion of the boundary-layer structure. The results are analyzed with emphasis placed on understanding how the freestream vortical structures cause modulation of the wall shear stress.

Experimental Configuration

Wind-Tunnel Facility

The experiments were carried out in a low-speed wind tunnel shown in Fig. 1a. The wind tunnel features extensive flow conditioning, sound muffling, and vibration isolation. The test section is square with 41 cm on a side at the inlet. A slight divergence of the side walls keeps the pressure gradient nominally zero. A plate divides the test section, which is 188 cm in length. A trip wire, 1.6 mm in diameter, is mounted 9 cm from the leading edge to ensure a uniform turbulent boundary layer. The flow into the test section has a turbulence intensity (u'/U_∞) of 0.2% and is free of swirl.

The experimental configuration is shown schematically in Fig. 1b. The interaction of both positive and negative circulation vortices were measured for three vortex generator heights. The vortex generator height controls the degree to which the vortices interact with the test plate leading edge and subsequent boundary layer.

The vortex generator (hereafter referred to as the "flap"), consisting of a wing that spans the tunnel, is mounted 24 cm in front of the leading edge. The flap is 2 cm in chord and resembles a symmetric airfoil in cross section with its maximum thickness near the leading edge. The large aspect ratio of the flap helps to minimize three-dimensional effects on the centerline of the test section. The flap is directly coupled to a dc servo motor (PMI U9M4Ha-2) on one side and is supported by a free pin on the other. The pivot point is near the leading edge. An optical encoder (PMI M-23) mounted on the motor shaft provides feedback of the motor position to a digital control system with a resolution of 0.045 deg. To generate the dynamic stall vortices in this experiment the flap moves from 0 to 13.5 deg and back in 25 ms (minus 13.5 deg generates a negative circulation vortex); this results in a reduced frequency ($\omega c/2U_\infty$) of 0.42 for the flap. The digital control system consists of a Galil digital motion control card (DMC) that is mounted in the laboratory's IBM PC/AT computer. The repeatability of the flap motion is critical to this experiment since ensemble averaging is required to resolve the unsteady flow. Comparing several measured motion profiles showed that the shaft positions never varied between realizations by more than 0.1 deg.

Data Acquisition and Reduction

The inlet conditions of the test section are monitored using a pitot static probe and a thermistor probe. The temperature in the laboratory varied by less than 2°C over the course of an experiment, which was typically 6 h in duration. To correct for any temperature variations we have adopted a modified form of the calibration scheme of Cimbala and Park.[9] The temperature calibration was carried out over a range of 5°C.

The two-dimensional velocity field was measured with a DISA P61 x-wire probe. The x-wire probe is well suited for the current investigations, since the mean flow is two dimensional with a maximum flow angle of 25 deg to the freestream direction. The wire sensors are copper-plated tungsten wire with an active diameter

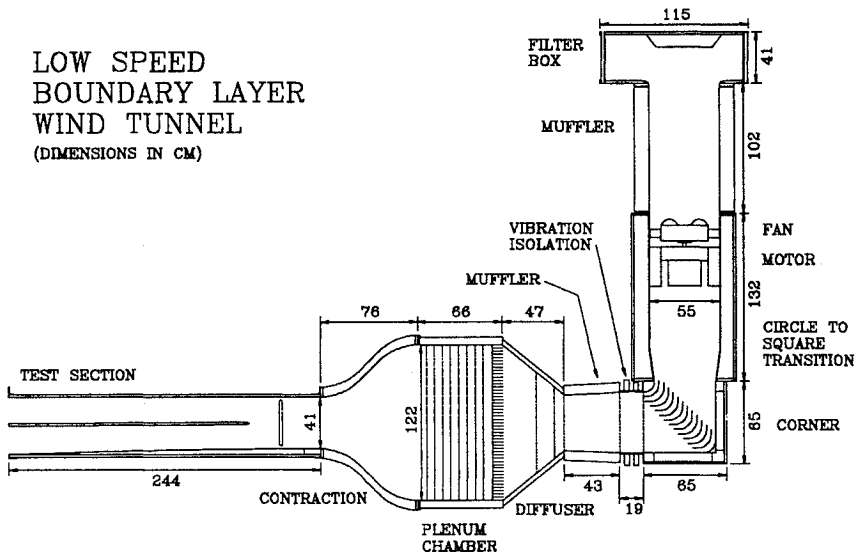

Fig. 1a Wind-tunnel facility.

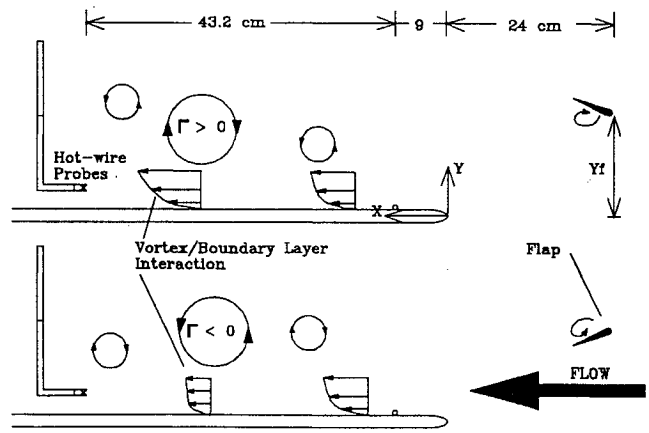

Fig. 1b Experimental configuration showing the two dynamic-stall vortex cases.

of 3 M and an active length of approximately 1 mm. The x-wire probe is operated at constant temperature with two DISA 55M10 bridges. The cutoff frequency after the dynamic balancing of the bridges is 20 kHz. The bridge voltages are measured, after applying a dc offset, with a Metra Byte DAS20 data acquisition board and an SSH-4 sample and hold board. The hot-wire calibration was checked before and after each experiment over a speed range of 2–12 m/s. The rms agreement between the pre- and postcalibrations was always better than 2% and typically in the range of 0.5–1.0%. The bridge voltages were sampled at a rate of 4 kHz per channel. Angular calibration of the x wire was carried out using the method described by Westphal and Mehta.[10] The steady boundary layer was thoroughly investigated before the unsteady experiments using 1000 samples acquired over a 2-s sample period.

A boundary-layer-type single-wire probe (DISA 55P05) was used to acquire unsteady measurements near the wall consisting of surveys at 55 vertical locations with 100 ensembles each. This number of realizations produced good convergence of the unsteady mean. At $x = 32$ cm the steady (undisturbed) boundary layer was found to be fully developed by the wake function criterion developed by Coles as reported by Purtell et al.[11] The single-wire measurements provided important information about the near-wall flow that was not accessible with the x wire.

Wall shear stress measurements were made with a hot wire (boundary layer type) positioned in the viscous sublayer at $y^+ < 3$. The single wire was calibrated at $x = 52$ cm to directly measure wall shear stress over a range of levels. The steady wall shear stress was obtained by taking a series of boundary-layer profiles and then determining the wall shear stress from log-law fits of the data. This shear stress was tabulated vs the local dynamic head and the data were then used as a standard for calibration of the single-wire placed adjacent to the wall. This technique is similar to the "wire on the wall" technique reported by Alfredsson et al.[12] The advantage of using a single-wire probe over fixing a wire to the wall, as done by Alfredsson et al., is that it can be easily moved. The distance from the wall was determined using a positioning telescope with a calibrated reticle. The measurement technique yields both the unsteady mean and turbulent fluctuating wall shear. For the steady boundary layer the ratio of the fluctuating wall shear to the mean shear was found to be 0.36, which is in good agreement with the value (0.40) reported by Alfredsson et al.[12]

The experiments were controlled using a computer to coordinate the flap motion with the data acquisition. The measurements reported are composed of time series describing the development of the unsteady flowfield after the vortex generation. Between each realization of the flap motion a 3-s pause occurred to ensure that the control system and flowfield came to equilibrium. The control system and actuation sequence was described in detail by Kothmann and Pauley.[13]

Kothmann and Pauley[13] studied the issues of data reduction of unsteady hot-wire data. They found that applying a low-pass (frequency domain) filter to the unsteady data was not feasible since there is substantial overlap between the frequencies that describe the unsteady mean flow and the turbulence. They concluded that ensemble averaging was the only viable method for resolving the unsteady mean and turbulent quantities in this flow. The unsteady mean flow $U(x, y, t)$ is calculated using ensemble averaging as

$$U(x, y, t_i) = \frac{1}{N} \sum_{n=1}^{N} u_n(x, y, t = t_i) \tag{1}$$

where N is the number of realizations. The ensemble-averaged turbulence quantities are determined as (for example)

$$\overline{u'^2}(x, y, t_i) = \frac{1}{N} \sum_{n=1}^{N} u_n^2(x, y, t = t_i) - U^2(x, y, t = t_i) \tag{2}$$

The unsteady mean flow and turbulence quantities were calculated at each time of the 512 point time series record for each probe position. For purposes of measuring the wall shear stress using the wall wire, the number of realizations of each event was increased to 500 since the run time is greatly reduced for a single probe position experiment.

Steady Flow

The steady, two-dimensional boundary-layer flow conditions are documented in Table 1 for the test plate without the vortex generator in the tunnel. The vortex generator wake, in its two lower positions, caused a slight thickening of the steady turbulent boundary layer. The wake, at its centerline, had a velocity defect relative to U_∞ of 3.2% at $x = 32$ cm.

Flowfield Description

Flow visualization was an important tool in this experiment for making qualitative assessments of the effect of the generator height and the general features of the unsteady flow. Since each realization of the unsteady flow involves a movement from rest of the vortex generator, a starting vortex was generated. The starting vortex had a sign opposite that of the dynamic-stall vortex. In addition, a vortex of the opposite sign followed the dynamic-stall vortex. This trailing vortex is a stopping vortex or what Gad-el-Hak and Ho[14] call a trailing-edge shedding vortex. These additional vortices that interact with the main vortex have an important effect on the velocity field and skin friction response.

In the following discussion the term "positive vortex case" refers to experiments in which a dynamic-stall vortex with positive circulation was generated (see upper half of Fig. 1b).

Figures 2a and 2b are smoke visualization photographs of the vortex boundary-layer interaction for the negative vortex cases at $x = 18$ cm with the vortex generator at $Y_f = 1.5$ and 1.1. The region between the starting and main vortices exhibits common flow toward the wall, and the stronger main vortex induces the starting vortex

Table 1 Steady flow conditions

x, cm	δ_{99s}, cm	δ_1, cm	δ_2, cm	$Re_{\delta 2}$	C_f
31.2	1.27	0.188	0.131	477	0.0057
52.2	1.6	0.271	0.193	704	0.0049

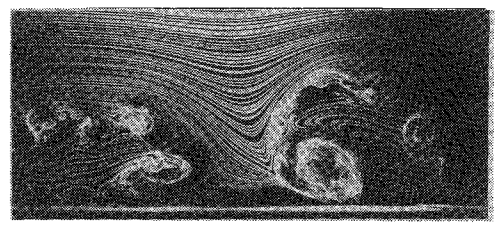

a) Negative case, $Y_f = 1.5$

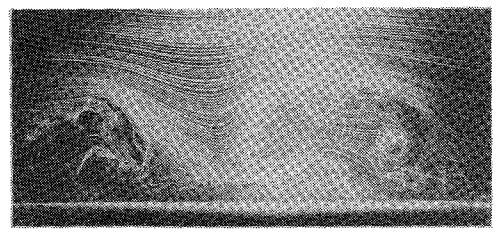

b) Negative case, $Y_f = 1.1$

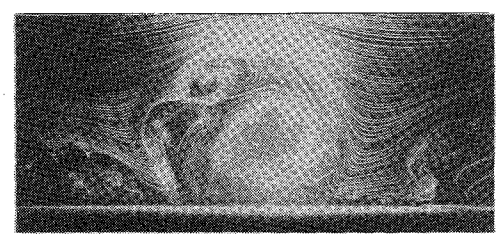

c) Positive case, $Y_f = 1.1$

Fig. 2 Flow visualization at $x = 18$ cm.

toward the wall. The $Y_f = 1.1$ case (Fig. 2b) is the strongest leading-edge interaction possible that still results in a coherent vortex. Here the vortex appears less coherent than the one shown in Fig. 2a by the time it reaches $x = 18$ cm. In general for the negative vortex cases, as the main vortex is brought closer to the surface, it is dissipated more quickly. A third case that was run with $Y_f = 2.0$ supports this trend.

Shown in Fig. 2c is the positive vortex case at $Y_f = 1.1$. The main vortex induces a flow in front of it directed away from the wall, causing the starting vortex to be lifted away from the wall. A negative stopping vortex follows behind the main positive vortex with a region of common flow toward the wall located between them. The results reported here are for the positive vortex case with the closest interaction, since it produced the strongest boundary-layer response. The responses for the positive vortex cases with a greater distance from the wall were similar in form.

Unsteady Velocity Field and Shear Stress

One of the objectives of this investigation was to relate the unsteady velocity field in the outer flow to the wall shear stress fluctuations caused by the vortex passage. The outer flow can be described by spanwise vorticity contours. The spanwise component of vorticity was calculated using measured convection velocities to estimate the x derivative:

$$\Omega_z = \frac{\partial V}{\partial x} - \frac{\partial U}{\partial y} \simeq -\frac{1}{U_c}\frac{\partial V}{\partial t} - \frac{\partial U}{\partial y} \tag{3}$$

The x-wire data sets at $x = 10$, 32, and 52 cm consist of vertical (y-direction) surveys of 35–40 points. In this paper the results at $x = 32$ cm will be presented. The vortex was first characterized at a location $x = -10.8$ cm, upstream of the test plate leading edge, for both cases. Upstream of the plate the circulation of the dynamic-stall vortices was estimated from an integration of the vorticity using the profile through the center of the vortex. The circulation was found to be 1060 and -1420 cm^2/s for the positive and negative cases, respectively. To evaluate the derivatives of ensemble-averaged unsteady mean velocity U and V were fit using cubic splines, applying a small amount of smoothing. The smoothing was such that the rms difference between the spline and the data was always less than 1%. The vorticity data are presented as contour plots with the axes representing the distance normal to the surface (y/δ_{99s}) and a coordinate that approximates the streamwise coordinate $x \sim t^*U_\infty$. The contour plots show the locations and strengths of the vortices. The convection velocities of the vortices were estimated using the time of arrival of the vortex centers at the three streamwise stations. The convection rate for the negative main vortex ranges from $U_c/U_\infty = 0.85$ at $Y_f = 1.1$ to $U_c/U_\infty = 0.93$ for $Y_f = 2.0$. With the positive vortex $U_c/U_\infty = 0.97$ for $Y_f = 2.0$ and did not vary significantly with vortex generator height. It must be emphasized that the contours do not represent an instantaneous picture of the flow but rather assume a "frozen field" behavior over a short distance. This method of presentation was discussed by Homa et al.[15] in their study of propagating vortices interacting with small bodies.

The spanwise vorticity contours are useful in comparing the three cases just discussed (Figs. 2a–2c) at $x = 31.2$ cm. In Fig. 3a the main negative vortex is well defined at $t^*U_\infty = 60$ with its center located at $y/\delta_{99s} = 2.0$. The starting vortex is in front of the main vortex, with its center at a streamwise location of 48 cm and a height of $y/\delta_{99s} = 2.0$. A positive secondary vortex follows closely behind the main negative vortex. In Fig. 3a the main negative vortex is located at the outer edge of the boundary layer, whereas in Fig. 3b it is fully embedded in the boundary layer. For the closest interaction case (Fig. 3b) the main vortex is not clearly defined in terms of vorticity contours, and it has lost most of its strength due to close interaction with the wall before reaching the measurement station. The secondary vortex that follows the main vortex appears to be more concentrated when the negative main vortex is closer to the surface.

For the positive vortex case, shown in Fig. 3c, the main vortex did not come into as close contact with the boundary layer as observed for the negative vortex cases. It was not possible to generate a positive vortex that was partially embedded in the boundary layer, but the positive vortices did modify the boundary layer significantly. The starting vortices observed for the positive cases are different

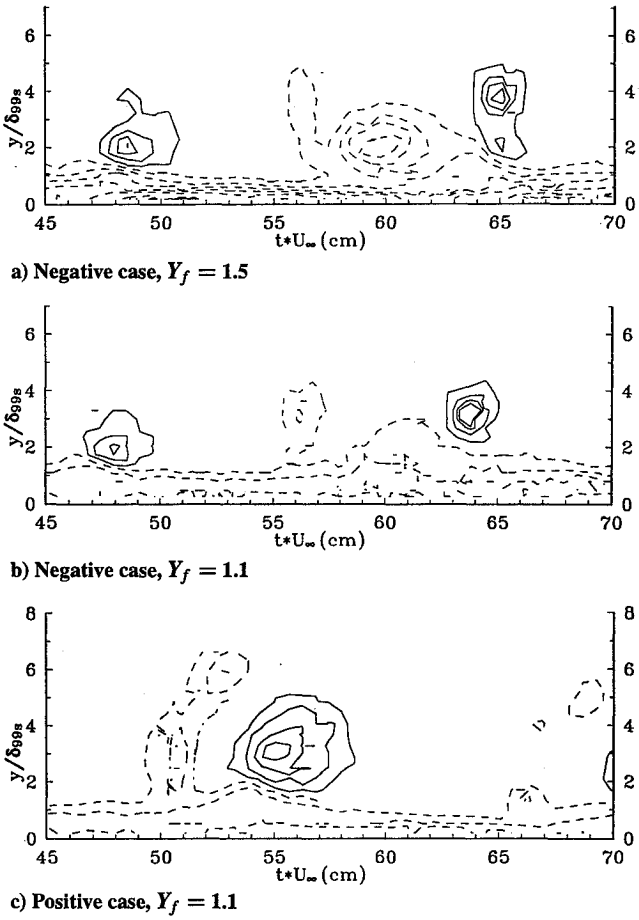

Fig. 3 Vorticity contours at $x = 32$ cm, levels: 20, 60, 100, 140, 185, and 300, solid line = positive, dashed line = negative.

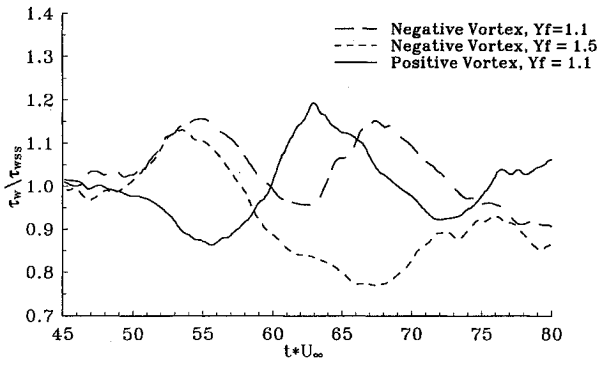

Fig. 4 Wall shear stress traces at $x = 32$ cm.

from those that occur in the negative cases. Because of the direction of rotation of the main vortex, these vortices are lifted away from the surface. As in the negative vortex cases discussed earlier, there is a weakening of the main vortex when it is in closer proximity to the surface, however, this weakening is not as severe in the positive vortex case.

Wall shear stress traces, normalized by their steady value, which correspond to Figs. 3a–3c, are presented in Fig. 4. The normalization removes small biases in the absolute levels that are caused by uncertainty in probe positioning (6% bias error in the worst case). The large number of ensembles (500) used for the wall shear measurements results in a 95% confidence interval of ± 2.9% random error for the unsteady mean values.

For the negative vortex cases, a positive change in the wall shear begins shortly after the positive starting vortex center passes. This is followed by a decrease caused by the passage of the main negative vortex. In the case with greater height above the wall (Fig. 3a) the negative peak in the wall shear occurs substantially after the passage of the main vortex center. The vortex center coincides with the

maximum perturbation in the streamwise velocity. The lag between passage of the vortex center and the peak shear stress for the $Y_f = 1.5$ case is $\Delta t^* U_\infty \approx 6$.

There is a significant difference between the negative $Y_f = 1.1$ case and the $Y_f = 1.5$ case. The large negative excursion in wall shear, which corresponds to the passage of the main negative vortex, is diminished for the closest interaction case. This is consistent with the observation made earlier based on flow visualization that in this case the main vortex has largely dissipated by the time it reaches $x = 32$ cm. A strong positive peak in wall shear caused by the trailing vortex was observed in the closest interaction case ($Y_f = 1.1$). This increase in wall shear begins at $t^* U_\infty = 62$, corresponding closely to the passage of the trailing vortex.

For the case with a positive main vortex a strong positive increase in the wall shear is associated with the passage of the main vortex. Similar to the negative vortex case ($Y_f = 1.5$), a phase lag between the arrival of the vortex center and the peak wall shear is indicated. Only a small decrease in the wall shear occurs between the starting vortices and the main vortex, indicating the weak influence of the starting vortices.

The streamwise pressure gradient was calculated from the ensemble-averaged x-wire data with the x derivative estimated using the convection velocity of the main vortex:

$$-\frac{1}{\rho}\frac{\partial p}{\partial x} \approx \frac{\partial U}{\partial t} - \frac{1}{U_c}\frac{\partial U}{\partial t} + V\frac{\partial U}{\partial y} \tag{4}$$

The third term was found to be significant in regions where the vortices induce a flow away from the wall ($V > 0$). These regions of positive V occur on the upstream side of the positive vortices and on the downstream side of the negative vortices. Since $\partial U/\partial y > 0$ at the boundary-layer edge for all times at $x = 32$ cm the third term in Eq. (4) primarily contributed to negative pressure gradients away from the vortex centers where V is the strongest. Figure 5 shows a comparison of the nondimensional pressure gradient ξ calculated with Eq. (4) for the three cases. For all cases the pressure gradient was calculated at the edge of the steady boundary layer ($y \approx 1.27$ cm). The pressure gradient has been made nondimensional with the steady values of boundary-layer thickness and wall shear stress. For steady boundary layers, values of $\xi = 6$ are mildly adverse, whereas $\xi < -5$ are considered to be strongly favorable according to White.[16] For both of the negative vortex cases (Figs. 3a and 3b), the positive starting vortices that pass the measurement station at $t^* U_\infty = 48$ cause a negative pressure gradient as they pass. The same is true of the positive main vortex that is centered on $t^* U_\infty = 55$ (Fig. 3c). The main negative vortex for $Y_f = 1.5$ shows a different characteristic from the positive vortices in that the pressure gradient changes sign near the vortex center at $t^* U_\infty = 60$. Secondary vortices of negative circulation also showed this characteristic. For the positive main vortex, the peak in negative pressure gradient (or favorable gradient) occurred at $t^* U_\infty = 56$, which corresponds to the peak in U_e and the vortex center as indicated by vorticity contours (Fig. 3c). The associated wall shear stress response does not peak until $t^* U_\infty = 63$. For the main negative vortex case with $Y_f = 1.5$, the peak positive pressure gradient (or adverse pressure gradient) occurs at $t^* U_\infty = 59$ and then quickly changes sign at a favorable pressure gradient. The wall shear stress response shows a steady decrease from the peak caused by the passage of the starting vortex at $t^* U_\infty = 55$ until 66. Hence the wall shear stress continued to decrease during the time period of $t^* U_\infty = 60$–67, whereas the pressure gradient was favorable. Comparisons of the pressure gradient compared with the wall shear stress indicate that the wall shear is not responding in phase with the pressure gradient (at $y/\delta_{99s} \approx 1$). This suggests that the pressure gradient felt in the near-wall region is not as strong as that measured/calculated at $y/\delta_{99s} \approx 1$, particularly for the negative vortex cases, where the vortex is partially embedded in the boundary layer.

Figure 6 shows the ensemble-averaged U velocity traces (from x-wire measurements) at four heights from outside the boundary layer to the edge of the inner layer for the negative vortex case, $Y_f = 1.5$. The main vortex causes a minima in U as it passes at $t^* U_\infty = 59.5$ corresponding to the vortex center (Fig. 3a). This minima occurs at the same time through the entire outer portion of the boundary

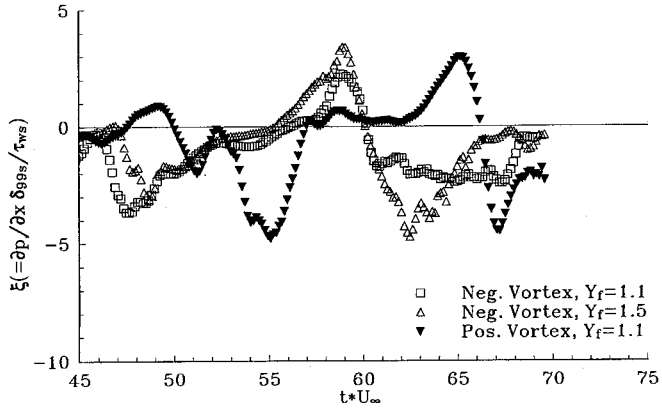

Fig. 5 Calculated pressure gradients at $x = 32$ cm.

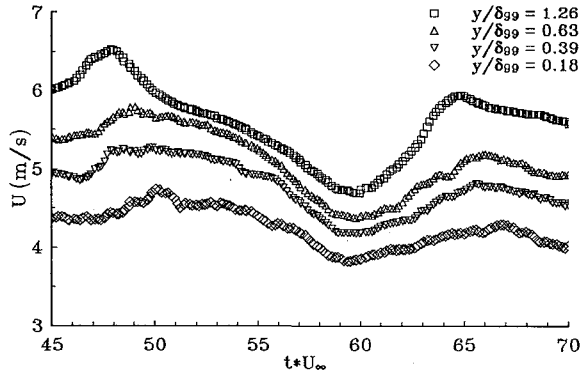

Fig. 6 Traces of ensemble-averaged U for $Y_f = 1.5$, negative case at $x = 32$ cm.

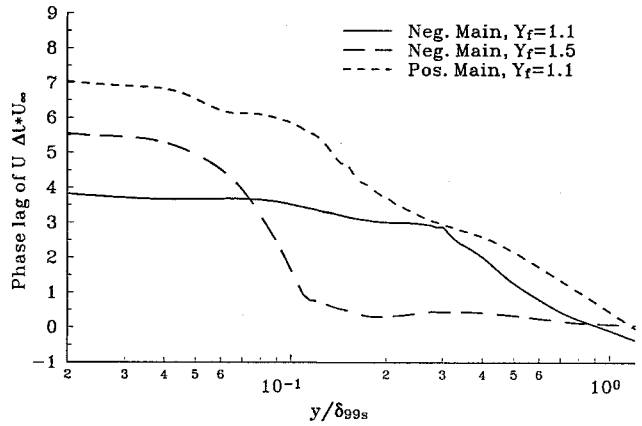

Fig. 7 Boundary-layer profiles of phase lag of ensemble-averaged U.

layer. This indicates that the vortex has a deep penetration into the boundary layer.

Using the single-wire measurements, profiles of the phase lag of U in response to the main vortex disturbance were assembled for each case. Figure 7 shows the results for the three cases here. The main difference between the positive vortex case ($Y_f = 1.1$) and the negative case ($Y_f = 1.5$) is the way the lag is spread across the boundary layer. The negative case shows stronger influence through the outer portion of the boundary layer, whereas the positive case has its phase lag spread partly across the outer layer, indicating that it has not penetrated the boundary layer to the same extent as the negative case with $Y_f = 1.5$. Phase lag profiles for other heights (not shown) were consistent with the preceding comparison, the exception being the negative case with $Y_f = 1.1$, which has a very weak main vortex at $x = 32$ cm.

The scaling of ensemble-average profiles of U using wall units and fitting the profile to the standard overlap region log law is discussed next. The velocity scale u^* that was determined from

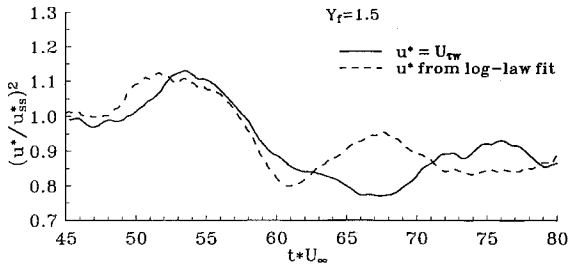

a) Negative case, $Y_f = 1.5$

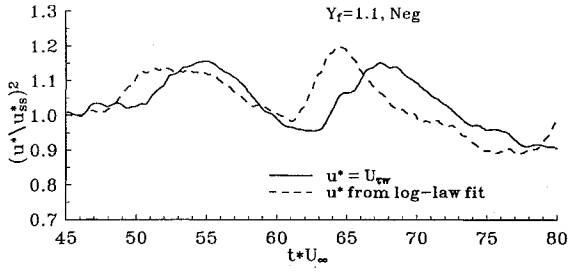

b) Negative case, $Y_f = 1.1$

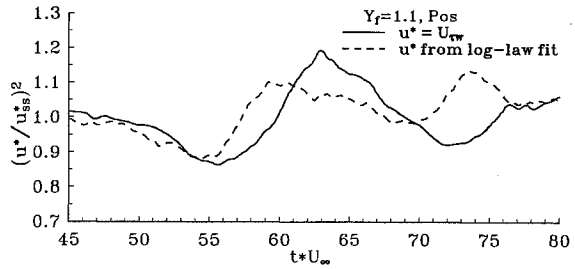

c) Positive case, $Y_f = 1.1$

Fig. 8 Traces of u^* (log-law fit) and $U_{\tau w}$.

a least squares analysis of the standard log-law equation: $U/u^* = 1/\kappa\, \ell n(y^*u^*/\nu) + B$ with $\kappa = 0.41$ and $B = 5.2$. The limits for the fits were set at $y^+ = 40$ and $y/\delta_{99s} = 0.24$ consistent with the ranges for low-Reynolds-number turbulent boundary layers.[11] The number of data points that fell in the range of the fit was at least eight. The rms error resulting from the fit was typically 1–2%. Figures 8a–8c show a comparison of u^{*2} with $\tau_w/\rho (= u^2_{\tau w})$. The results show that u^* is similar to $u_{\tau w}$ but there is a phase difference. The phase difference is such that the u^* is always leading, and this indicates that the stress in the overlap region is leading the stress at the wall. This is consistent with the results in Fig. 7, which showed how the phase lag is distributed across the boundary layer. For the main negative vortex case with $Y_f = 1.5$, the phase was concentrated entirely in the region $y/\delta_{99s} < 0.1$, and therefore this case should demonstrate a large difference in phase between the wall stress velocity scale and that indicated by the log law, u^*. The results in Fig. 8a show the minima associated with the main vortex to be out of phase by approximately the same magnitude as the total phase lag indicated in Fig. 7 ($\Delta t^* U_\infty = 6$). Similarly from Fig. 8c the phase difference between the two velocity scales due to the main positive vortex is approximately the same as the phase lag in U across the inner region of the boundary layer. The results indicate that the velocity scale u^* in the overlap region has a phase lead over the friction velocity that is similar to the phase lead of the U velocity response in the outer boundary layer over that in the inner layer. Although the two velocity scales are similar in magnitude and have similar responses, the results indicate that the use of wall functions to calculate unsteady boundary-layer flows is not completely justified. A similar conclusion has been reached in investigations of oscillating (standing wave) boundary layers.[17] If the scaling velocity in the overlap region u^* is based on the turbulent shear stress, then the results indicate that a significant phase lag in the response of the turbulent shear stress exists across the inner region. In the next section we present measurements of ensemble-averaged turbulent stresses.

Response of Turbulent Stresses

The results discussed earlier demonstrate that the passage of the vortex structures cause significant modulations of the mean flow in the near-wall region. Further understanding of the near-wall flow is possible by examining the response of turbulent stresses through the boundary layer during these modulations. Profiles of the turbulent stresses through the boundary layer for the negative vortex case with $Y_f = 1.5$ only are presented at key times in the interaction.

The turbulence quantities have a higher uncertainty than the mean flow for the number of samples used. The 95% confidence interval, based on 100 samples, for the turbulence normal stresses (u'^2, v'^2) is $\pm 33\%$. For this reason the ensemble-averaged turbulence quantities were filtered by averaging over five adjacent time bins and then assigning that value to the central bin. This effectively reduces the 95% confidence interval to $\pm 6\%$ while decreasing the temporal resolution. Good temporal resolution is still obtained due to the high sampling rate used in obtaining the original samples. This filtering was found to reduce the scatter in the data while maintaining the features of the dynamic responses.

Figures 9a–9c show profiles of $\overline{u'^2}$ across the boundary layer before the vortices arrive ($t^* U_\infty = 30$), at minimum U_e (60), and at the minimum wall shear stress (66). Here we use profiles measured with the single wire to include the near-wall flow. The three profiles show three distinct levels of turbulent kinetic energy in the outer

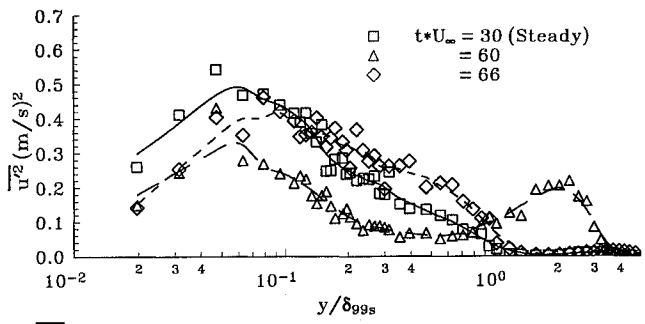

a) $\overline{u'^2}$

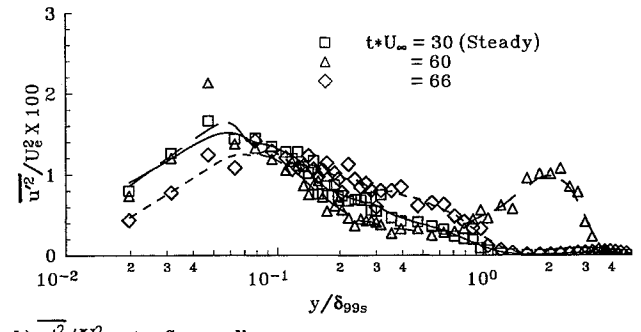

b) $\overline{u'^2}/U_e^2$ outer flow scaling

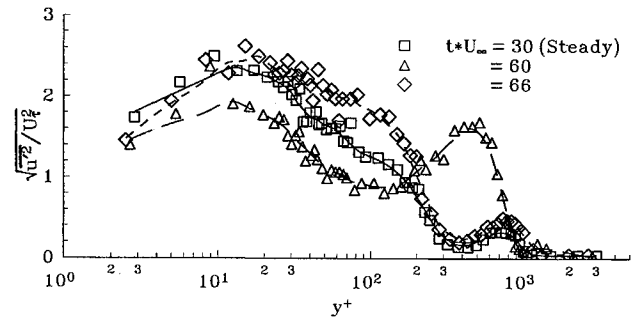

c) $\sqrt{\overline{u'^2}}/U_{\tau w}$ inner flow scaling

Fig. 9 Profiles of ensemble-averaged turbulent normal stress u'^2, negative case, $Y_f = 1.5$, at $t^* U = 30$, 60, and 66.

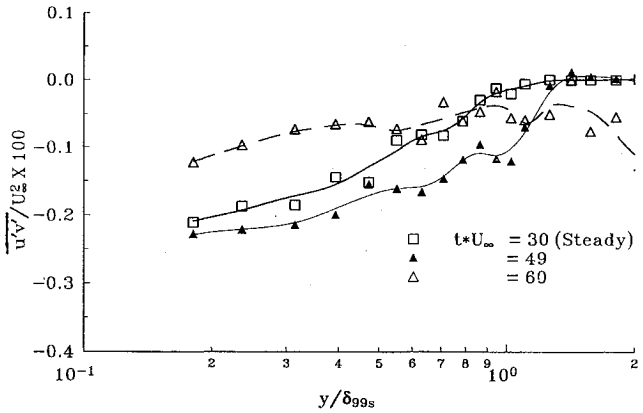

a) t^*U_∞ = 30 (steady), 49 (starting vortex), and 60 (main vortex)

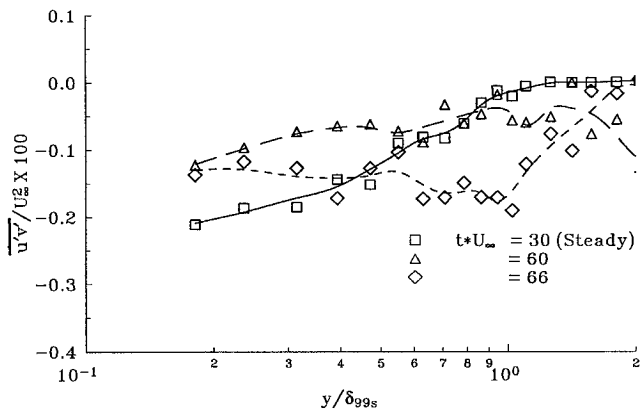

b) t^*U_∞ = 30 (steady), 60 (main vortex), and 66 (min. wall shear)

Fig. 10 Profiles of ensemble-averaged turbulent shear stress, $\overline{u'v'}$, negative case, Y_f = 1.5.

part of the boundary layer. In particular as the main negative vortex arrives at $t^*U_\infty = 60$ the levels are low relative to the steady flow over the entire boundary layer. Note the profile is shown beyond the boundary layer and the presence of the turbulent main vortex is clearly evident at 60. At the time of the arrival of the main vortex center (60), the fluid in the outer layer has experienced a reduced level of shear ($\partial U/\partial y$) and thus reduced shear stress production of $\overline{u'^2}$. In addition in the region between the starting vortex and the main vortex $\partial U/\partial x > 0$ so that normal stress production term will reduce $\overline{u'^2}$. For $t^*U_\infty = 66$ the conditions are the opposite in terms of shear and normal stress production, thus the levels of kinetic energy are relatively higher in the outer flow. The inner layer, however, shows reduced levels relative to the steady flow profile at 66.

Figures 9b and 9c show the same profiles as Fig. 9a but normalized by inner and outer quantities, respectively. In Fig. 9b the ensemble-averaged U_e was used; this brings the three profiles closer together in the outer region ($y/\delta_{99s} > 0.2$). However, they are not completely collapsed. Figure 9c shows the profiles in wall units with the wall shear stress determined from the direct measurements discussed in Fig. 4. Wall unit normalization clearly improves the collapse of profiles in the near-wall region while amplifying their differences in the outer region. Normalized profiles generated for the positive vortex case showed a similar trend. The results indicate that the primary normal stress $\overline{u'^2}$ has an unsteady response similar to the mean flow, although some phase difference is evident due to the lack of complete collapse of profiles on ensemble-averaged (unsteady) mean quantities. The results of Samson et al.[4] indicate similar trends at low reduced frequencies in periodic turbulent boundary layers.

In Figs. 10a and 10b profiles of the turbulent shear stress $\overline{u'v'}$, measured with the x wire are shown. The x-wire measurements cannot reach the inner region of the boundary layer in this experiment. Figure 10a shows that the turbulent shear stress was generally increased in magnitude across the outer region of the boundary layer at the arrival time of the positive vortex ($t^*U_\infty = 49$) and decreased as the main negative vortex arrives (60) relative to the steady profile (30). In Fig. 10b profiles at $t^*U_\infty = 60$ (main negative vortex center) with the profile at the time of minimum shear stress. The trend of the profiles as the inner region is approached indicates that at $t^*U_\infty = 66$ the turbulent shear stress is reduced in magnitude over that at 60 in the inner region. These trends are consistent with the wall shear stress measurements, that is, whereas the wall shear stress is greatly reduced at 60 relative to the steady values, the minimum occurs at a later time (66). Near the edge of the boundary at 66 the turbulent shear level is increased dramatically, indicating a significant phase difference (lag) between the inner and outer layers.

Conclusions

A thorough investigation of the velocity field and wall shear stress for a class of spanwise vortex boundary-layer interactions has been presented. Both positive circulation and negative circulation vortices were measured at three different heights above a flat plate test surface. One focus of the results has been on relating the outer flow disturbances, as described by vorticity, and pressure gradient to the wall shear stress responses. It is shown that the passage of a positive circulation vortex results in an increase in the wall shear, and the passage of a negative circulation vortex results in a decrease in wall shear. In all cases a single peak in the wall shear stress lags the passage of the vortex center. The effect of vortex height on wall shear stress was strongest for the negative circulation cases where the vortices were partially or fully embedded in the boundary layer. A comparison of the calculated pressure gradient with the wall shear stress showed them to be out of phase for the positive case. For the negative case, with $Y_f = 1.5$, which is partially embedded in the boundary layer, the pressure gradient as calculated has little direct effect on the wall shear.

A scaling velocity u^* was determined from the near-wall profiles by applying the standard log-law equation, which describes the overlap region in steady turbulent boundary layers. The term u^* was found to lead the friction velocity determined from direct measurement of the wall shear but was similar in magnitude and form of response.

Turbulent stresses were determined from the ensemble-averaged data. Profiles of $\overline{u'^2}$ were scaled using outer and inner velocity scales. The scaling was partially successful in collapsing the profiles in the outer region when U_e was the scale, and similarly in the inner region when $u_{\tau w}$ was used. This indicates that the turbulent normal stresses do not respond completely in phase with the local mean flow. Profiles of ensemble-averaged turbulent shear stress $\overline{u'v'}$ measured through the outer portion of the boundary layer indicate a similar trend as the wall shear stress.

Acknowledgment

The authors gratefully acknowledge the financial support of the Office of Naval Research (Contract N00014-89-J-3102).

References

[1]Ashworth, D. A., LaGraff, J. E., and Schultz, D. L., "Unsteady Interaction Effects on a Transitional Turbine Blade Boundary Layer," *ASME Journal of Turbomachinery*, Vol. 111, 1989, pp. 162–168.

[2]Hancock, P. E., and Bradshaw, P., "Turbulence Structure of a Boundary Layer Beneath a Turbulent Free Stream," *Journal of Fluid Mechanics*, Vol. 205, 1988, pp. 45–76.

[3]Brereton, G. J., Reynolds, W. C., and Jayaraman, R., "Response of a Turbulent Boundary Layer to Sinusoidal Free-Stream Unsteadiness," *Journal of Fluid Mechanics*, Vol. 221, 1990, pp. 131–160.

[4]Samsom, G. L., Johnson, W. A., and Cook, W. J., "Hot Wire Measurements of Reynolds Stresses in a Boundary Layer Generated by a Periodic Free-Stream Flow," FED-Vol. 167, Thermal Anemometry-1993, American Society of Mechanical Engineers, 1993.

[5]Patel, M. H., "On Turbulent Boundary Layers in Oscillatory Flow," *Proceedings of the Royal Society of London*, Vol. 353, 1977, pp. 121–144.

[6]Evans, R. L., and Yip, R. S. K., "An Experimental Investigation of Unsteady Wake-Boundary-Layer Interaction," *Journal of Fluids and Structures*, Vol. 2, 1988, pp. 313–322

[7]Nelson, C. F., Koga, D. J., and Eaton, J. K., "Unsteady, Separated Flow Behind an Oscillating, Two-Dimensional Spoiler," *AIAA Journal*, Vol. 28, No. 5, 1990, pp. 845–852.

[8]Gursul, I., and Rockwell, D., "Vortex Street Impinging Upon an Elliptical Leading Edge," *Journal of Fluid Mechanics*, Vol. 211, 1990, pp. 211–242.

[9]Cimbala, J. C., and Park, W. J., "A Direct Hot-Wire Calibration Technique to Account for Ambient Temperature Drift in Incompressible Flow," *Experiments in Fluids*, Vol. 8, 1990, pp. 299, 300.

[10]Westphal, R. V., and Mehta, R. D., "Crossed Hot-Wire Data Acquisition and Reduction System," NASA TM 85871, Jan. 1984.

[11]Purtell, L. P., Klebanoff, P. S., and Buckley, F. T., "Turbulent Boundary Layer at Low Reynolds Number," *Physics of Fluids*, Vol. 24, No. 5, 1981, pp. 802–811.

[12]Alfredsson, H. P., Johansson, A. V., Haritonidis, J. H., and Eckelmann, H., "The Fluctuating Wall Shear Stress and the Velocity Field in the Viscous Sublayer," *Physics of Fluids*, Vol. 31, No. 5, 1988, pp. 1026–1033.

[13]Kothmann, B. D., and Pauley, W. R., "Interaction of Unsteady, Turbulent, Vortical Structures with a Turbulent Boundary Layer," AIAA Paper 92-0060, 1992.

[14]Gad-el-Hak, M., and Ho, C.-M., "Unsteady Vortical Flow Around Three-Dimensional Lifting Surfaces," *AIAA Journal*, Vol. 24, No. 5, 1986, pp. 713–721.

[15]Homa, J., Lucas, M., and Rockwell, D., "Interaction of Impulsively Generated Vortex Pairs with Bodies," *Journal of Fluid Mechanics*, Vol. 197, 1988, pp. 571–594.

[16]White, F. M., *Viscous Fluid Flow*, 2nd ed., New York, 1991, Chap. 6.

[17]Cousteix, J., and Houdeville, R., "Turbulence and Skin Friction Evolutions in Oscillating Boundary Layers," *Turbulent Shear Flows*, Springer–Verlag, Berlin.